Published OnlineFirst January 12, 2018; DOI: 10.1158/1078-0432.CCR-17-2733

Biology of Human Tumors

Clinical Cancer Research

Personalized RNA Medicine for Pancreatic Cancer

Maud-Emmanuelle Gilles[1], Liangliang Hao[2,3,10], Ling Huang[4], Rajesha Rupaimoole[1], Pedro P. Lopez-Casas[5], Emilia Pulver[2,3], Jong Cheol Jeong[1,6], Senthil K. Muthuswamy[4], Manuel Hidalgo[4], Sangeeta N. Bhatia[2,3,7,8,9,10], and Frank J. Slack[1]

Abstract

Purpose: Since drug responses vary between patients, it is crucial to develop pre-clinical or co-clinical strategies that forecast patient response. In this study, we tested whether RNA-based therapeutics were suitable for personalized medicine by using patient-derived-organoid (PDO) and patient-derived-xenograft (PDX) models.

Experimental Design: We performed microRNA (miRNA) profiling of PDX samples to determine the status of miRNA deregulation in individual pancreatic ductal adenocarcinoma (PDAC) patients. To deliver personalized RNA-based-therapy targeting oncogenic miRNAs that form part of this common PDAC miRNA over-expression signature, we packaged antimiR oligonucleotides against one of these miRNAs in tumor-penetrating nanocomplexes (TPN) targeting cell surface proteins on PDAC tumors.

Results: As a validation for our pre-clinical strategy, the therapeutic potential of one of our nano-drugs, TPN-21, was first shown to decrease tumor cell growth and survival in PDO avatars for individual patients, then in their PDX avatars.

Conclusions: This general approach appears suitable for co-clinical validation of personalized RNA medicine and paves the way to prospectively identify patients with eligible miRNA profiles for personalized RNA-based therapy. *Clin Cancer Res; 24(7); 1734–47. ©2018 AACR.*

Introduction

Pancreatic ductal adenocarcinoma (PDAC) is a highly aggressive cancer with a very poor prognosis that progresses rapidly. Multiple therapeutic trials developed to date, such as with chemotherapy, radiation, and antistromal therapies, have only resulted in small advances, and survival after diagnosis is generally less than a year (1). Clearly, novel therapeutics based on a better understanding of this disease combined with new drug delivery systems are desperately needed. Here, we tested a preclinical strategy with a novel RNA-based therapeutic tool for personalized PDAC treatment.

miRNAs are small (~18–25 nucleotides) RNAs that can bind target mRNAs in a sequence-specific fashion to induce their posttranscriptional downregulation. Several studies have already identified miRNAs with significantly altered expression between normal pancreas and PDAC tissues; among them, one of the more relevant is miR-21 (2–5). Our laboratory previously generated a mouse model of miR-21 overexpression and revealed that the mice develop tumors in the tissue where miR-21 is overexpressed and that the tumors depend on the continued expression of miR-21 for their survival (6). In addition, our group has already proposed a novel antimiR delivery platform that effectively inhibits oncomiR-155 in another mouse model introducing a new paradigm in the use of antimiRs as anticancer drugs (7). These lines of evidence highlight the role of "oncomiR addiction" in maintenance of the tumor phenotype in cancer and open avenues for new therapeutic options (8).

Pancreatic cancer is hypovascularized and largely not penetrable, making therapeutic drug delivery a current challenge (9, 10). RNAs are often large and charged, preventing them from easy internalization in the cell. In addition, instability in circulation and rapid renal clearance make the delivery of small RNAs to the tumor site particularly difficult (11). Previous studies testing direct miRNA-based therapy for pancreatic cancer in mouse models have used viral-based vectors, prior antimiR transfection of tumor cells before inoculation to mouse models, or delivery through intratumoral injection (12–16). To date, direct use of antimiRs has failed to target miRNAs *in vivo* in PDAC (12). We hypothesized that targeted nanoparticles encapsulating oligonucleotide analogues will reduce the rapid clearance of antimiRs and

[1]Harvard Medical School Initiative for RNA Medicine, Department of Pathology, Cancer Center, Beth Israel Deaconess Medical Center, Harvard Medical School, Boston, Massachusetts. [2]Institute for Medical Engineering and Science, Massachusetts Institute of Technology, Cambridge, Massachusetts. [3]Koch Institute for Integrative Cancer Research, Massachusetts Institute of Technology MIT, Cambridge, Massachusetts. [4]Beth Israel Deaconess Medical Center, Cancer Center, Department of Medicine, Harvard Medical School, Boston, Massachusetts. [5]Spanish National Cancer Research Centre (CNIO), Madrid, Spain. [6]The division of Biomedical Informatics, The Department of Internal Medicine, College of Medicine, The University of Kentucky, Lexington, Kentucky. [7]Department of Medicine, Brigham and Women's Hospital and Harvard Medical School, Boston, Massachusetts. [8]Broad Institute of Massachusetts Institute of Technology and Harvard, Cambridge, Massachusetts. [9]Howard Hughes Medical Institute, Cambridge, Massachusetts. [10]Marble Center for Cancer Nanomedicine, Massachusetts Institute of Technology, Cambridge, Massachusetts.

Note: Supplementary data for this article are available at Clinical Cancer Research Online (http://clincancerres.aacrjournals.org/).

Corresponding Author: Frank J. Slack, Beth Israel Deaconess Medical Center, 330 Brookline Ave, Boston, MA 02215. Phone: 617-735-2601; Fax: 617-735-2646; E-mail: fslack@bidmc.harvard.edu

doi: 10.1158/1078-0432.CCR-17-2733

Published OnlineFirst January 12, 2018; DOI: 10.1158/1078-0432.CCR-17-2733

increase their delivery and internalization into the PDAC tumor site to prevent the growth of PDAC tumors. In this new strategy, we used nanoparticles containing "tandem" peptides combining a cell-penetrating peptide transportan and tumor-penetrating peptide iRGD (17–19) that have been previously shown to deliver siRNAs to the tumor site in a model of ovarian tumor (20). This particle complexes with RNA through charge and hydrophobic interactions to form tumor-penetrating nanocomplexes (TPN; ref. 21). Because iRGD has been recently demonstrated to enhance delivery and biodistribution of chemotherapy in PDAC (22), we tested the efficacy of TPNs in the delivery of antimiRs to PDAC.

It is accepted that there is a strong disconnect between preclinical work performed in cell lines and xenografts and success of clinical trials (23). For this reason, we tested our miRNA-based therapeutic on patient-derived-xenograft (PDX) samples and patient-derived-organoids (PDO) to better capture human tumor heterogeneity and potentially predict patient response. In our study, through encapsulation in TPN, we successfully delivered antimiR therapeutics to the tumor site for PDAC. We show, for the first time, the potential for a new therapeutic precision medicine strategy that monitors levels of oncomiRs in individual patient tumor samples and that tests RNA-based therapeutic nano-drugs in patient avatars to predict future clinical response in pancreatic cancer.

Results

Clinically relevant oncomiRs form part of a tumor signature in human PDAC patient samples

To identify a PDAC miRNA signature, we worked with an initial set of 27 PDAC snap-frozen tumor samples from PDXs that maintain tumor architecture and clonal diversity (24, 25). This set has known gemcitabine resistance status (24) and *KRAS* mutation status (Supplementary Table S1A). To determine miRNA expression patterns in PDAC tumors, we conducted a Firefly microRNA assay of our PDAC set compared with 3 normal pancreatic samples. For these assays, 46 miRNAs already known to be associated with *KRAS*, with pancreatic cancer, or similar diseases were preselected and profiled from our PDAC samples (Supplementary Table S1B). Associated bioinformatics analysis of our profiling revealed the deregulated miRNA expression profile of PDX samples compared with normal samples presented as a heatmap of fold change (Fig. 1A; Supplementary Fig. S1A). An ANOVA test comparing control samples with PDX tumor samples revealed 9 miRNAs significantly deregulated with an adjusted $P \leq 0.01$ (dark dot; miR-217 is out of volcano plot) and additional 4 miRNAs significantly deregulated with raw $P \leq 0.01$ (blue dot; Fig. 1B).

To functionally validate the oncomiR signature revealed by the PDAC tumor sample analysis, we developed PDAC 3D models, which formed compact and round spheroids after 7 to 8 days in culture (Fig. 1C). We also generated human tumor organoids from 5 independent PDX tumors (Panc 286, Panc 281, Panc 219, PDO 030, and PDO 017) that we characterized and used later as an additional PDAC model for functional tests (Figs. 5 and 6). Firefly microRNA assay was performed on PDAC cell lines, 3D cultures models, and PDO to analyze their miRNA signature (Supplementary Fig. S1B). Interestingly, an ANOVA test comparing all tumor samples (cell lines, 3D models, and PDO) with control samples (including normal pancreatic cell lines and pancreatic organoid from normal early progenitor) revealed that 6 miRNAs (miR-21-5p, miR-146a-5p, miR-196a-5p, miR-196b-5p, let-7i-5p, and miR-29b-5p) from the 13 significantly deregulated miRNAs from PDX profiling are consistently upregulated between PDX and cell line/organoids profiles (Fig. 1D). This group of 6 miRNAs forms part of a PDAC signature and reveals a list of potent PDAC oncomiRs that are commonly upregulated in both PDX cell lines and PDO models. Additional data from a set of 191 patients (prognostic miRNA database; ref. 26) showed that of these 6 oncomiRs, high miR-21, 196a, 196b, and let-7i expression levels in patients are strongly associated with low survival in pancreatic cancer (Fig. 1E) and reveal miR-21-5p, miR-196a, and miR-196b as a significant potential clinically relevant regulators of PDAC initiation and progression and key miRNAs to detect and target in PDAC using an RNA-based medicine approach.

OncomiR inhibition limits PDAC 3D model growth

To test the therapeutic potential of oncomiR inhibition for personalized PDAC therapy for the remainder of this study, we selected one of the 4 oncomiRs that emerged from our analysis above. We chose to first focus on miR-21-5p for our "proof-of-concept" study as it has previously been reported to be prognostic in PDAC (27) and because from this set of patient tumor samples, PDAC cell lines, and organoids, it is part of 8 miRNAs (miR-21-5p, let-7b-5p, let-7a-5p, let-7c-5p miR-22-3p, miR-30b-5p, miR-103-3p, and miR-92-3p) found in relative high abundance. First of all, overexpression of miR-21-5p via the firefly profiling was confirmed in all of the PDAC models by qRT-PCR (Supplementary Fig. S2A).

Analysis of each tumor sample's miR-21-5p expression showed that all the 27 tumor samples upregulated miR-21-5p (Fig. 2A), which we confirmed by qRT-PCR (Fig. 2B). To support the relevance of this miR-21-5p profile, we tested mRNA expression for two PDAC miR-21-5p direct targets, the tumor supressors programmed cell death 4 (*PDCD4*) and phosphatase and tensin homolog (*PTEN*) in these PDX samples (28). *PDCD4* and *PTEN* mRNA expression in tumor samples revealed a significant inverse correlation with miR-21-5p expression for *PDCD4* as well as a strong tendency toward downregulation for *PTEN* (Fig. 2C and D), supporting a key role played by the oncomiR miR-21-5p in PDAC. To investigate the role of miR-21 in PDAC growth, we functionally inhibited miR-21-5p by generating a GFP-stable cell line where miR-21 activity was inactivated via a LentimiRa-Off-hsa-miR-21-5p (Lenti-21). Loss of activity of miR-21 was validated by measuring the rescue of mRNA expression of miR-21 targets, including *PDCD4* and *PTEN* (Supplementary Fig. S2B), compared with a Lenti-empty vector control.

Lenti-transduced cells were plated to promote spheroid formation as for Fig. 1C and their relative growth rate studied. Interestingly, whereas cells transduced by the lentivirus control (Lenti-control) grew with the same kinetics as untransfected cells, Lenti-21 spheroids showed a decrease in spheroid number and in size (Fig. 2E). Metabolic activity measurements of these 3D cultures showed that miR-21 inhibition decreased 3D viability by 50%, suggesting that miR-21 inhibition may promote PDAC cell death (Fig. 2F). To validate this idea, we stained for apoptosis by using a specific dye that is cleaved in the nucleus under high levels of activated caspase-3. Analysis of the staining showed a

Published OnlineFirst January 12, 2018; DOI: 10.1158/1078-0432.CCR-17-2733

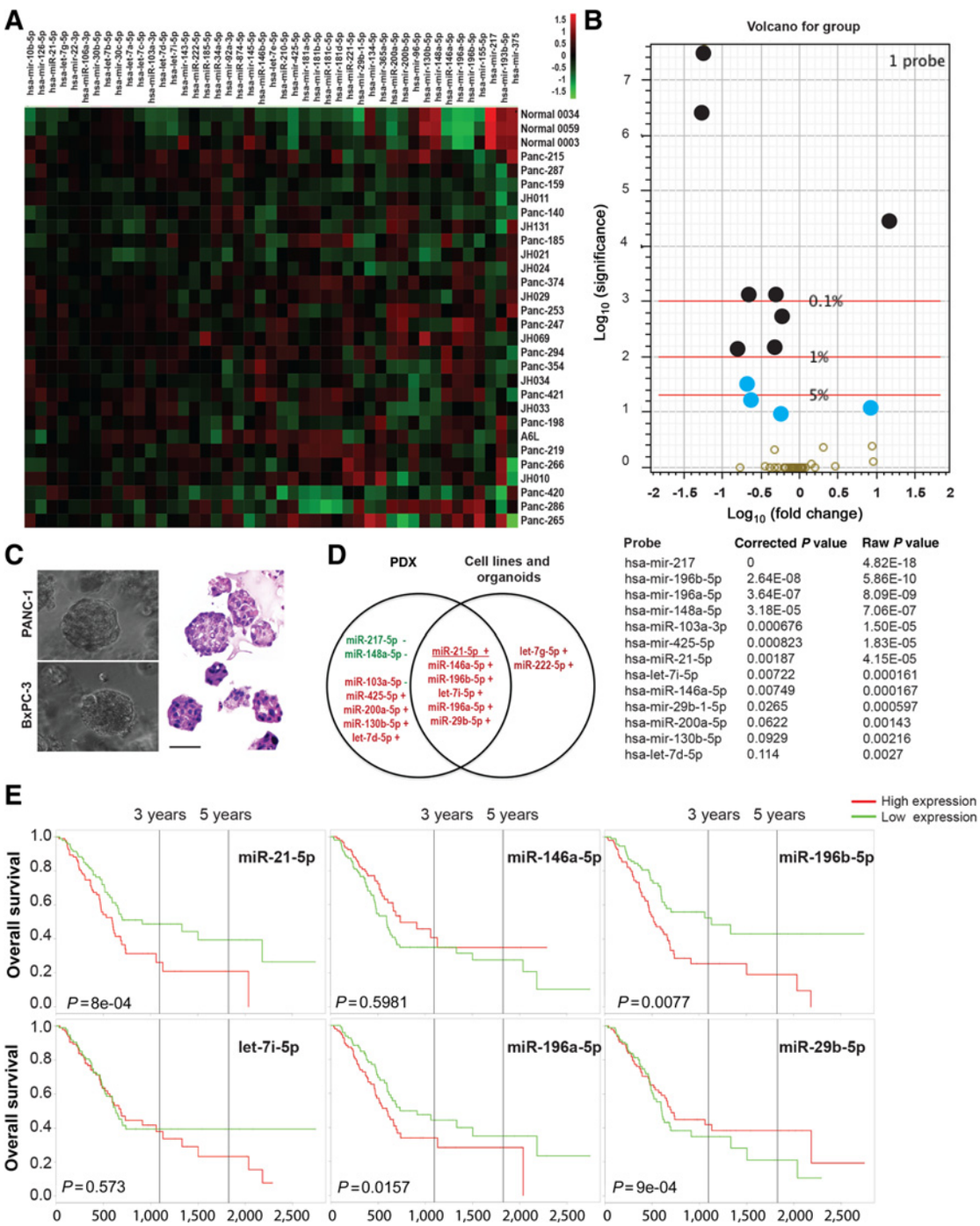

Figure 1.

A, A heatmap of miRNA expression in PDAC PDX tumor samples ($n = 27$ cases) compared with normal pancreas samples ($n = 3$ control). Normalized miRNA signal intensities are presented as fold change (log_{10} of the ratio between a probe value to the average of all the other samples for that probe). Green, highly expressed miRNA; red, lowly expressed miRNA. miRNA profiling was done through the firefly circulating miRNA assay and normalized using two miRNAs that are not significantly deregulated between all samples, miR-22-3p and miR-30b-5p defined by the geNorm-like algorithm. **B,** Volcano plot of statistical significance against fold change between tumor samples group and normal samples group, demonstrating the most significantly deregulated miRNAs. Significantly deregulated miRNAs are classified by adjusted *P* value (black dot) and raw *P* value (blue dot; ≤0.01). **C,** Representative phase-contrast pictures of PDAC 3D sphere models from PANC1 and BxPC3 cell lines and PDO Panc 286 and Panc 281**.** Scale bar, 1,000 μm. **D,** Overview of the top commonly deregulated miRNAs from PDX and cell line/organoid profiling. The list of miRNAs was generated by matching the 14 miRNAs significantly deregulated (≤0.01) from PDX profiling with the 14 miRNAs most deregulated (ranked by *P* value) from cell line–organoid profiling. miR-21-5p* is the only miRNA significantly upregulated in both profiling experiments: (+) is used for upregulated miRNAs and (−) for downregulated miRNAs. **E,** PROGmiR representation of miR-21-5p, miR-146a-5p, miR-196b-5p, let-7i-5p, miR-196a-5p, and miR-29b-5p expression and overall survival in pancreatic adenocarcinoma. High miR-21-5p, miR-196b-5p, let-7i-5p, and miR-196a-5p expression are clinically correlated with decreased overall survival in pancreatic cancer. *, $P = 0.01$–0.05; **, $P = 0.001$–0.01; ***, $P < 0.001$; ****, $P < 0.0001$; N.S., not significant, two-tailed *t* test.

Published OnlineFirst January 12, 2018; DOI: 10.1158/1078-0432.CCR-17-2733

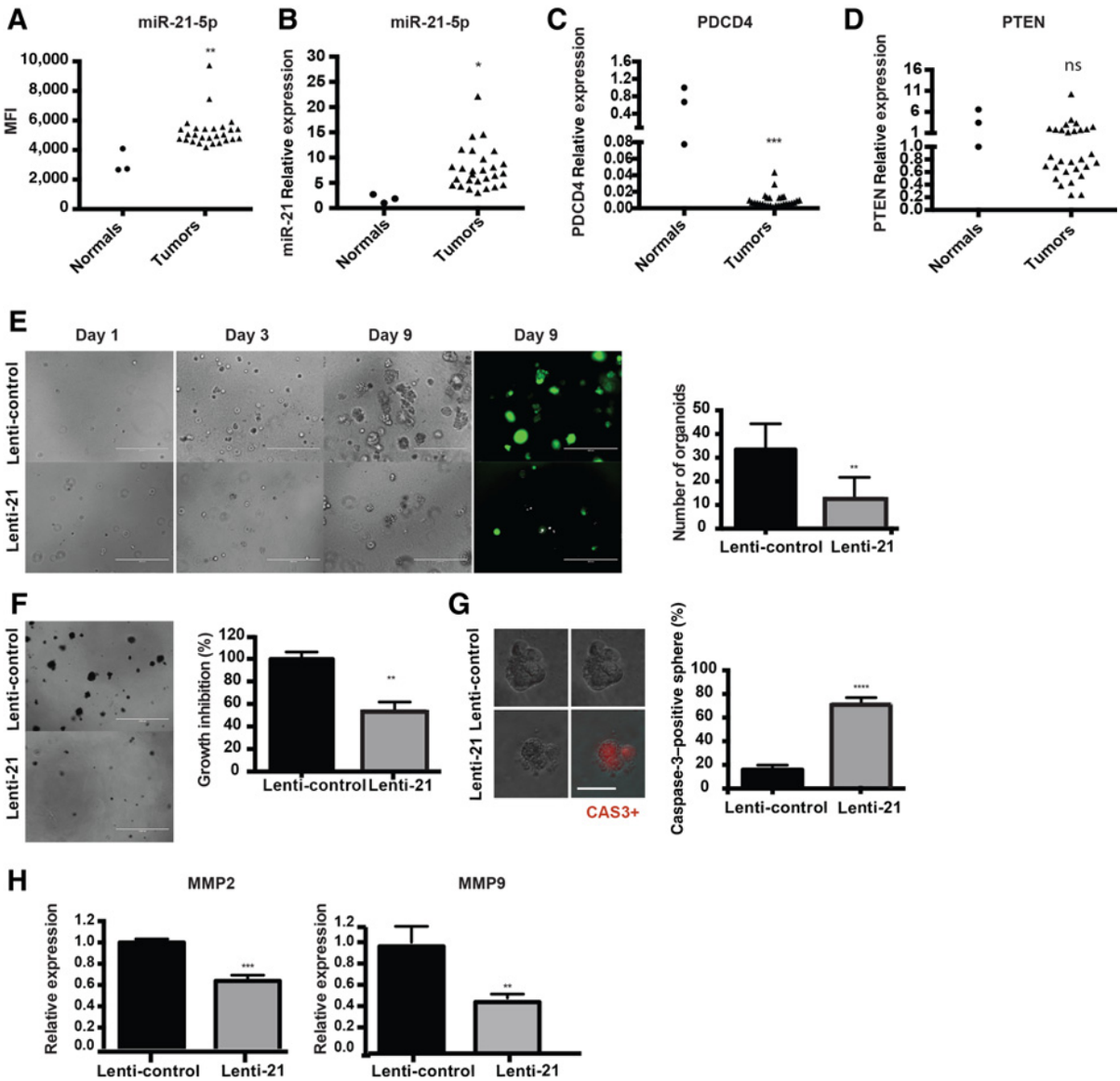

Figure 2.

A, Relative expression (mean of fluorescence) of miR-21-5p in the set of PDAC tumors compared with normal controls. **B,** qPCR analysis of miR-21-5p expression level in the set of PDAC tumors compared with normal controls with a dynamic range from 3- to 22-fold. **C** and **D,** qPCR analysis of PTEN and PDCD4 expression levels compared with normal controls. **E,** Growth kinetics of Lenti-21 3D model cells from day 1 to 9. Quantification of the number of organoids per well at the end of treatments. Scale bar, 400 μm. **F,** Cell metabolic activity measures from MTT assay at 9 days of 3D model growth and associated representative pictures. Scale bar, 1,000 μm. **G,** NucView staining (red) report significant increase in caspase-3 activity in Lenti-21 spheroids. Quantification of caspase-3–positive spheroids. **H,** qPCR of MMP-2 and MMP-9 expression level in PANC1 stable cell line (Lenti-21). For qPCR, each miRNA sample was normalized on the basis of both its U6 content and on the basis of GAPDH for mRNAs. Scale bar, 50 μm. Error bars, mean ± SD. *, $P = 0.01$–0.05; **, $P = 0.001$–0.01; ***, $P < 0.001$; ****, $P < 0.0001$; N.S., not significant, two-tailed t test; $n = 3$ biological replicates.

significant increase of the caspase-3 activity in the Lenti-21 spheroids at the end of the 9-day assay (Fig. 2G).

miR-21-5p has been previously described to promote pancreatic cancer cell invasion by indirectly increasing the mRNA expression of metalloproteinase-2 and 9 (29). We observed that PANC-1 transduced by Lenti-21 expressed a lower level of these two MMPs, supporting the PDAC growth delay phenotype in 3D culture (Fig. 2H; ref. 29).

Because it is currently not possible to inhibit miR-21 by transduction of a stable lentiviral construct for human therapy, we tested whether miR-21 inhibition by transfection of a *mir*Vana miRNA inhibitor would show similar effects in PDAC cells. In PANC-1, BxPC3, and PL-45, we obtained, respectively, 95.2%, 87.3%, and 64.6% decrease in miR-21 expression at the dose of 50 nmol/L (Supplementary Fig. S2C). The *mir*Vana miRNA inhibitor was used to inhibit miR-21 in the remaining

Published OnlineFirst January 12, 2018; DOI: 10.1158/1078-0432.CCR-17-2733

parts of our study. Through utilization of this anti–miR-21 strategy, we demonstrated that the targeting of relevant oncomiRs counteracts PDAC tumor progression and reveals the potent role of oncomiR inhibition.

TPNs promote potent delivery of RNA-based therapeutics to PDAC

To optimize delivery and targeting of RNA medicine therapeutic compounds to the tumor site, we encapsulated antimiRs in TPN that had been described to increase tumor targeting through sequential binding to integrins and NRP1 by tumor-penetrating peptide iRGD (20, 22). iRGD specifically binds to $\alpha_v\beta3$ integrins, and following proteolytic cleavage, initiates transcytosis and internalization through a semaphorin receptor NRP1 present on tumor cells (17, 30). TPN consists of a C-terminal cell-penetrating peptide iRGD and a N-terminal fatty acid group used to facilitate hydrophobic interactions for self-assembly of nanoparticles. Here, consistent with our prior approach, we selected anti–miR-21 RNA that self-associated with and condensed into nanoparticles, called TPN-21 (Fig. 3A). As it has already been described that cell-penetrating peptide transportan and tumor-penetrating peptide iRGD do not bind and penetrate in low integrins-NRP1 pancreatic cells *in vitro* and *in vivo* (18, 19, 21), we first validated the expression of the two binding proteins targeted by TPN-21 in PDAC cells by performing Western blots. Semiquantitative analysis of their expression showed that all the tumor cell lines expressed elevated levels of both receptors (integrins and NRP1), compared with normal pancreatic duct epithelial cell H6c7 (normalized to 1; Fig. 3B). This result indicated that iRGD-containing TPNs should specifically bind integrins/NRP1 positive PDAC tumor models as confirmed in Supplementary Fig. S3A. Next, we demonstrated the capacity of TPN-21 (100 nmol/L) administration without a transfection agent to inhibit miR-21 expression in PDAC cells at a comparable level to conventional anti–miR-21 transfection (50 nmol/L; Supplementary Fig. S3B).

To test TPN in a 3D PDAC model, we first validated the specific binding of the tumor-penetrating peptide (iRGD) in this context. PDAC spheres were incubated with iRGD-TAMRA for 2 hours and observed under a fluorescence microscope. We observed a strong red fluorescent signal on the sphere surface corresponding to iRGD-TAMRA binding after 2- to 4-hour incubation (Fig. 3C). In addition to surface binding, it was important to assay whether the TPNs could be internalized into the sphere. For this purpose, TAMRA-TPN delivery was monitored by confocal microscopy. Z-stack confocal images (Fig. 3D) revealed binding and lumen internalization of TPN-21 (TAMRA-TPN-21) into spheres generated with two different PDAC samples.

As previously observed after targeting the stable cell lines to inhibit miR-21 (Fig. 2E), repeated administration of TPN-21 (100 nmol/L) following an every-other-day treatment plan (Supplementary Fig. S3C) reduced the number and size of 3D models of PDAC (Fig. 3E). Analysis of miR-21 expression by qRT-PCR on treated spheres revealed a 70% knockdown of miR-21, indicating successful delivery and functional activity of the anti–miR-21 compound in the 3D model (Fig. 3F). It has already been described that use of tumor-penetrating peptide iRGD accumulates in a tumor-specific manner in PDAC (18). Here, to validate the *in vivo* homing behavior of iRGD-TPN-21, we generated a PDAC orthotopic model in mice and performed a single intravenous injection of TAMRA-TPN-21 allowing us to assay for TPN-21 fluorescence in mouse organs. Analysis of TPN-21 biodistribution 6 hours postinjection was performed by analyzing tissue fluorescence. As commonly found for nucleic acid delivery, after 6 hours, the highest fluorescent accumulation remains in the liver (31), but relatively high levels of fluorescence were also detected in the tumor site, compared with other organs from the reticuloendothelial system (spleen and lung; Fig. 3G). Altogether, these data suggest that iRGD-TPN-21 will promote pancreatic tumor–selective delivery of anti–miR-21 therapy to the PDAC tumor site.

RNA-based therapy reduces KC model tumor growth and restores PTEN and PDCD4 expression

To explore the clinical potential of the results observed in 3D models, we used a mouse model to test TPN-21 therapy efficiency *in vivo*. We first focused on the D8-175 mouse cell line (mPDAC) derived from Pdx1-Cre; Kras $^{LSL\text{-}G12D}$; Trp53 $^{fl/fl}$ (KPC) mice (32) that bear the most common mutations found in PDAC patients (*KRAS* and *TP53*). We demonstrated that mPDAC cells highly expressed the two TPN-21 receptors of TPN (integrins and NRP1; Fig. 3B). We observed an 80-fold upregulation of miR-21-5p by qRT-PCR in mPDAC compared with normal mouse pancreas (Fig. 4A). We also validated that use of anti–miR-21 promotes apoptosis on mPDAC cells by analyzing the costaining of active caspase-3 (apoptotic cells) and DAPI (total cells) and observed a 2-fold change in apoptotic rate after anti–miR-21 treatment (Fig. 4B).

To test whether use of RNA-based therapy can disrupt tumor maintenance and be a successful approach for PDAC patients, we first tested antimiR treatment through TPN-mediated delivery *in vivo*. We generated a PDAC mouse model by injection of 5×10^5 mPDAC cells/flank in NOD/SCID mice (Fig. 4C). Animals bearing mPDAC allograft were intravenously injected with TPN-control or TPN-21 (5 mg/kg of antimiR) 2 times per week over 36 days, starting when the tumor volume reached approximately 150 mm in diameter. Tumor size measurements revealed that delivery of anti–miR-21 significantly reduced mPDAC tumor growth after only 1 injection (Fig. 4D). As expected from our 3D analysis (Fig. 3E), repeated, systemic administration of the TPN-21 strongly slowed tumor growth along the entire treatment course from day 1 to day 36 and resulted in a 51.1% suppression of tumor growth (15.07 vs. 30.83 relative tumor burden size vs. baseline) at the end of the treatment (Fig. 4E). Interestingly, tumor growth is most affected in the first 24 days of treatment with TPN-21 compared with TPN-control (4.25 vs. 14.37 relative tumor burden vs. baseline), suggesting a more potent effect of anti–miR-21 in the early stages of tumor growth.

To validate miR-21 targeting to the tumor site following TPN-21 therapy, mPDAC tumors were collected at the end of the treatment, and miR-21 expression was determined by qPCR. We found that miR-21 expression was significantly decreased in the mPDAC tumors group treated with TPN-21 compared with the mPDAC tumors group treated with TPN-control (Fig. 4F). As a consequence of miR-21 inhibition, we observed a significant restoration of miR-21 targets, PTEN and PDCD4 (Fig. 4G). Altogether, these data showed that use of TPN-21 allowed delivery of anti–miR-21 into the tumor site promoting inhibition of miR-21 expression and upregulation of tumor suppressor PTEN and PDCD4, which correlated with reduced tumor growth.

On the basis of our result, we demonstrate that use of TPN approach is suitable for safe and potent delivery of RNA-based therapy (antimiR oligonucleotides) compound to the tumor site.

Published OnlineFirst January 12, 2018; DOI: 10.1158/1078-0432.CCR-17-2733

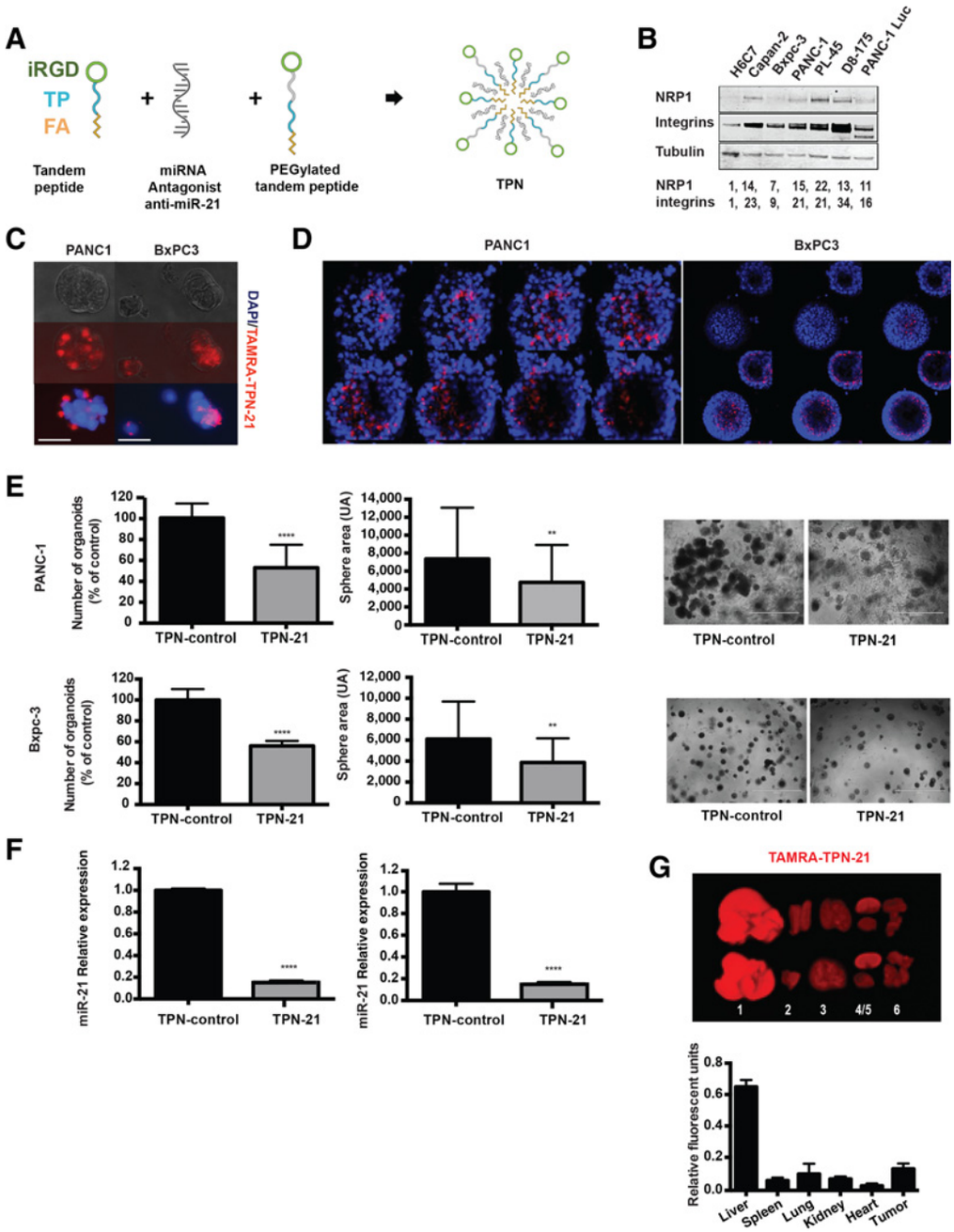

Figure 3.

A, Representation of TPN loaded with anti–miR-21 (TPN-21). **B,** Western blot analysis of two receptors (NRP1 and integrins) bound by the TPN. Column 1 (H6c7 normal pancreatic cell lines), columns 2–7 (PDAC human and mouse cell lines). Western blot band corresponding to NRP1 and integrins have been quantified against tubulin levels and normalized against normal cell lines (1). **C,** TAMRA-TPN-21 (red) binding in PDAC 3D models after 1 hour of treatment. Nuclei were stained with DAPI. Scale bars, 100 μm (PANC-1) and 50 μm (BxPC-3). **D,** Z-stack confocal images show binding of TAMRA-TPN-21 to the PANC1 and BxPC3 spheroid and internalization into the lumen after 2-hour treatment. **E,** Quantification of number and size of 3D sphere after TPN-21 treatment and representative picture of Bxpc3 and PANC1 3D models after repeated TPN-21 treatments. Sphere size was measured through imageJ software on a total of 35 spheroids and is presented in arbitrary units (UA). **F,** qPCR analysis of miR-21-5p expression level after TPN-21 treatment. **G,** Tumor biodistribution of fluorescent-TPN-21 in organs (1, liver; 2, spleen; 3, lung; 4, kidney; 5, heart) and tumor site (6, pancreas) after 48-hour injection in an orthotopic KC model of PDAC ($n = 2$). For qPCR, each miRNA sample was normalized on the basis of its 18s content and on the basis of GAPDH for mRNAs. Error bars, mean ± SD. *, $P = 0.01$–0.05; **, $P = 0.001$–0.01; ***, $P < 0.001$; ****, $P < 0.0001$; N.S., not significant, two-tailed t test; $n = 3$ biological replicates and $n = 2$ biological replicates for Western blot analysis.

Published OnlineFirst January 12, 2018; DOI: 10.1158/1078-0432.CCR-17-2733

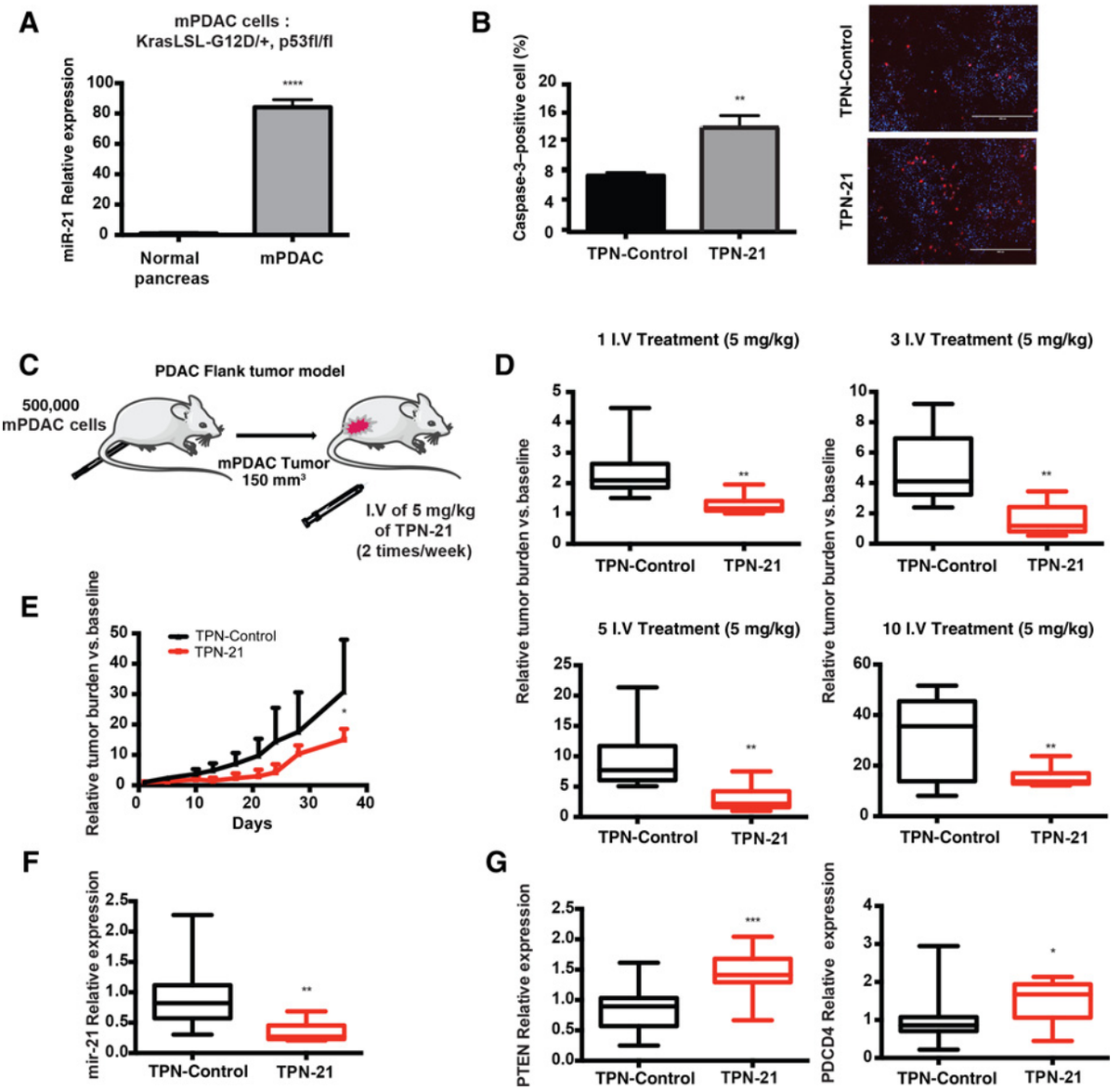

Figure 4.

A, qRT-PCR of miR-21-5p expression level in the PDAC (mPDAC) cell line compared with normal pancreas. **B,** Nucview staining (red) normalized to total cells stained with DAPI (blue) reports significant increase of the caspase-3 activity after TPN-21 treatment in mPDAC cells. **C,** mPDAC flank tumor model. **D,** Relative tumor burden after [1, 3, 5, and 10 intravenous injection of TPN-control $n = 7$ or TPN-21 $n = 10$ (5 mg/kg)]. **E,** Relative tumor burden after intravenous injection of TPN-control or TPN-21 (5 mg/kg) over the 36 days. **F,** qPCR analysis of miR-21-5p expression level in the tumor site at the end of treatment (TPN-control $n = 5$; TPN-21 $n = 5$). **G,** qPCR analysis of PTEN and PDCD4 expression level at the end of treatment (TPN-control $n = 5$; TPN-21 $n = 5$). For qPCR, each miRNA sample was normalized on the basis of its 18s content and on the basis of β-actin for mRNAs. Error bars, mean ± SD. *, $P = 0.01$–0.05; **, $P = 0.001$–0.01; ***, $P < 0.001$; ****, $P < 0.0001$; N.S., not significant, two-tailed t test; $n = 3$ biological replicates.

TPN-21 impacts human PDO growth and predicts PDX response

To study patient responses to the TPN-21 strategy, we generated human tumor organoids from PDX tumors. We selected one patient sample that has been studied extensively and shows a high degree of concordance between the human sample biopsy and the biopsy growing in mice (24). In addition, this PDX has been characterized as gemcitabine resistant (Supplementary Table S1B) with a poor therapeutic outcome. To generated PDO 286, fresh PDX tumor fragments were minced and processed accordingly to protocol (33) and grown in Matrigel (Fig. 5A). These organoids formed as multilayers of cells with diameters between 50 and 150 μm. They were largely filled with tumor cells, but also exhibited the presence of microlumens. The general morphology of organoids shown by H&E resembled the tumor tissues *in vivo* (Fig. 5B). In addition, we showed by IHC that PDO 286 expressed both TPN receptors (Fig. 5B). Before testing our RNA-based strategy

Published OnlineFirst January 12, 2018; DOI: 10.1158/1078-0432.CCR-17-2733

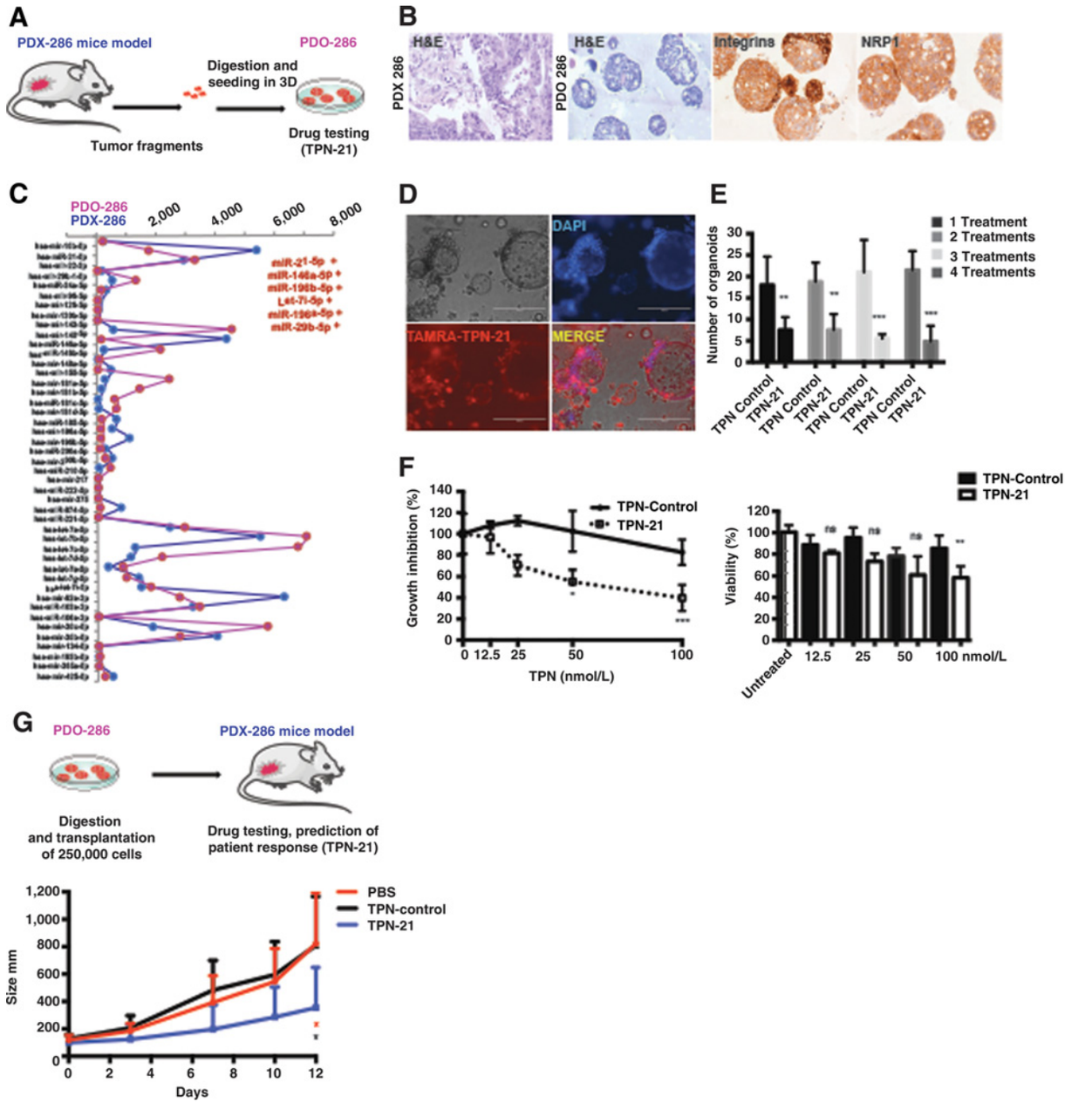

Figure 5.

A, Representation of PDO 286 and PDX-286 model. **B,** Representative H&E pictures of PDX-286 and PDO 286. IHC staining for two tumor-penetrating receptors (NRP1 and integrins) on PDO 286. **C,** Overview of miRNA expression profile of PDO 286 and PDX-286. The list of miRNAs was generated by considering only the 6 miRNAs highly deregulated from both profiling experiments (Fig. 2B). These 6 miRNAs are commonly upregulated (+) in both PDX and PDO, relative to their own control (normal pancreas for PDX profiling) and (normal organoid for PDO profiling). **D,** TAMRA-TPN-21 binding in PDO 286 after 1 hour of treatment. Nuclei were stained with DAPI. TAMRA-TPN-21 is red. Scale bar, 400 μm. **E,** Number and size of PDO 286 after treatment by TPN-21 or TPN-control (1, 2, 3, and 4 treatments) at the optimum dose of 100 nm. Dose–response curve of PDO 286 treated with TPN-21 or TPN-control compared with untreated organoids (doses are 0, 12.5, 25, 50, and 100 nmol/L). **F,** Cell metabolic activity measured from MTT assay at 9 days of 3D culture growth. **G,** Representation PDX-286 generation from PDO 286. Tumor size of the PDX after intravenous injection of PBS ($n = 6$), TPN-control ($n = 6$) or TPN-21 ($n = 5$; 5 mg/kg) over the 13-day treatment and representative pictures of PDX tumors after treatments with PBS, TPN-control or TPN-21. *, $P = 0.01$–0.05; **, $P = 0.001$–0.01; ***, $P < 0.001$; ****, $P < 0.0001$; N.S., not significant, two-tailed t test.

on PDO, we first validated that the general miRNA profile was maintained between this PDX and this PDO. By statistically analyzing the miRNA profile of PDX 286 and PDO 286, we observed a general concordance of miRNA expression levels, with strong correlations (Spearman $\rho = 0.75$) and high statistical significance ($P = 2.7e\text{-}8$) between the two samples (Fig. 5C). We also validated that the most deregulated miRNAs from both profiles (miR-21-5p, miR-146a-5p, miR-196b-5p, let-7i-5p,

Published OnlineFirst January 12, 2018; DOI: 10.1158/1078-0432.CCR-17-2733

miR-196a-5p, miR-29b-5p; Fig. 1D) are also commonly upregulated in PDO 286 relative to their own control (Fig. 5C).

To investigate the binding and internalization of TAMRA-TPN into the PDO, PDO 286 was incubated with TAMRA-TPN for 2 hours and observed under a fluorescence microscope. We validated that the fluorescent peptide bound 90% of the organoids after 2 hours (Fig. 5D). To test TPN-21 on this patient avatar, we performed repeated administration of TPN-21 (100 nmol/L) following an every-other-day treatment plan (Supplementary Fig. S3C). We counted the number of organoids growing per well at days 3, 5, 7, and 9 of treatment. A delay in organoid growth was apparent after only 1 treatment, reaching a maximum effect at 9 days (Fig. 5E). This observation showed that TPN-21 induced a strong inhibitory effect on tumor growth starting from early times of the treatment course as we previously observed with the mouse cell line *in vitro* (Fig. 4D and E). We also verified in this PDO model that miR-21 expression was reduced at the end of treatment (Supplementary Fig. S4A). Then, we performed a dose–response study by treating PDO with TPN-21 or TPN-control for 9 days at different concentrations (12.5, 25, 50, and 100 nmol/L) following the same every-other-day treatment plan (Supplementary Fig. S3C). We observed that repeated administration of TPN-21 significantly decreased the number of organoids per well from the dose of 25 nmol/L compared with TPN-control, whereas at the 100 nmol/L dose, we observed a decrease of 50% in the number of organoids (Fig. 5F). In parallel, we performed a metabolic activity measure by using MTT on the organoids, which confirmed significant inhibition of their viability (42%) after 4 repeated administration of 100 nmol/L TPN-21 (Fig. 5F).

To verify that use of the PDO predicts specific patient response to TPN-21 *in vivo*, we generated a PDX with the cells from Panc-286 PDO to test effects of repeated injection of TPN-21 on PDX tumor growth (Fig. 5G). Six-week-old nude mice were injected with 250,000 cells from PDO 286. When the tumor volumes reached the size of around 100 mm^3, xenografts were intravenously injected with TPN-control or TPN-21 (5 mg/kg of compound) for a total of 4 injections, using the same schedule applied in the organoid assay. We included a PBS control group to validate that use of the TPN delivery system itself did not significantly impact tumor growth. As observed with PDO 286 (Fig. 5E), 4 repeated systemic administrations of TPN-21 strongly slowed tumor growth from day 1 to day 13 and resulted in 54.2% suppression of tumor growth (6.98 PBS vs. 6.19 TPN-control vs. 3.20 TPN-21 relative tumor burden vs. baseline) by the end of the treatments (Fig. 5G). Relative tumor burden versus baseline from PBS and TPN-control group are not significantly different at the end of treatment showing that use of TPN itself does not promote antitumor effects (Supplementary Fig. S4B). Altogether, these results showed that use of RNA-based oligonucleotides inhibits homogeneously PDO and PDX PDAC growth, highlighting the therapeutic potential of TPN-21 for human PDAC therapy. In addition, here, we showed that our approach consisting in utilization of PDAC patient avatars can be used as a rapid prescreen to systematically investigate patient's sensitivity to personalized RNA-based therapy.

PDO screen for personalized RNA-based therapy

Because we previously demonstrated that PDO and PDX maintained their general histologic characteristics and miRNA profiles (Fig. 5B and C) and because PDO can predict PDX responses (Fig. 5E–G), we decide to test whether we could predict the eligibility for TPN-21 therapy in 4 additional patients through rapid screening of their PDO avatars.

As we are developing TPN-21 strategy (by targeting miR-21-5p among the 4 key candidate miRNAs from our profiling), we started by evaluating the expression level of miR-21-5p in the 4 PDO at approximately 7 days by qPCR analysis. Among the 4 PDOs studied here, 2 overexpressed miR-21-5p compared with normal organoids, and 2 PDOs did not show overexpression at that stage (Fig. 6A). As previously performed in Fig. 5, repeated administration of TPN-21 (100 nmol/L) following an every-other-day treatment plan was performed on these new PDOs (Supplementary Fig. S3B). To measure the sensitivity of PDO to TPN-21, we performed a MTT assay to evaluate PDO viability, and we measured the size of the organoids at the end of the treatment. We found that only the 2 PDOs overexpressing miR-21 (PDO 286 and PDO 219) showed a significant growth delay after TPN-21 therapy (Fig. 6B–E).

In addition to the TPN-21 screen, we treated PDOs with the current standard of care for PDAC patients, gemcitabine. We used gemcitabine at the same dose as TPN-21 for this screen because in 4 cell lines tested for gemcitabine sensitivity, all showed an average IC_{50} of 117.25 nmol/L that is consistent with the range used for TPN-21 (data not shown). Here, gemcitabine treatment did not lead to a significant decrease in PDO 286 size or viability in the same dose range as TPN-21 (Fig. 6B), whereas PDO 219 was affected. In agreement with previous observations concerning the prevalence of gemcitabine resistance (Supplementary Table S1A), our data suggest the potential benefit of TPN-21 for gemcitabine-resistant patients. Consistent with another study combining anti–miR-21 and gemcitabine in PDAC, use of TPN-21 therapy sensitized resistant PDOs to gemcitabine treatment by reducing organoid size and viability (Supplementary Fig. S5A and 5B; ref. 34).

More interestingly, the 2 "low-miR-21" PDOs (PDO 030 and PDO 017) did not show sensitivity to TPN-21 therapy under these conditions (Fig. 6F–I). These results suggest that the patients (PDO/PDX) that do not overexpress miR-21 will potentially not respond to TPN-21 therapy. Altogether, these results demonstrate that a rapid screen of PDO is capable of evaluating and predicting patient response to TPN-21 therapy and suggest that miR-21 overexpression in patient samples could be used as a biomarker for predicting favorable outcome to TPN-21 therapy. In addition, our study conducted on PDX 286 and PDO 286 strongly suggests the favorable therapeutic potential of TPN-21 use for gemcitabine-resistant patients.

Discussion

RNA therapeutics for cancer, including anti–miR-21, have been discussed for the past few years, but their reported lack of delivery to most disease tissues has limited their therapeutic use to liver and kidney disease (35–37). The work described here demonstrates a targeted approach to deliver RNA-based therapy including antimiRs and potentially mimics, to a specific tumor type (PDAC) or tumor microenvironment where drug delivery is routinely poor. By packaging RNA-based oligonucleotides in TPNs targeting specific PDAC tumor receptors, we propose safe and efficient delivery of RNA therapy, paving the way for the use of TPN-21 as a therapeutic anticancer agent for PDAC. We demonstrated that TPN-21 strongly restrains PDO growth, even where gemcitabine failed, and limits PDAC growth *in vivo* (Figs. 5E–G and 6B). Currently, numerous personalized models that help

Published OnlineFirst January 12, 2018; DOI: 10.1158/1078-0432.CCR-17-2733

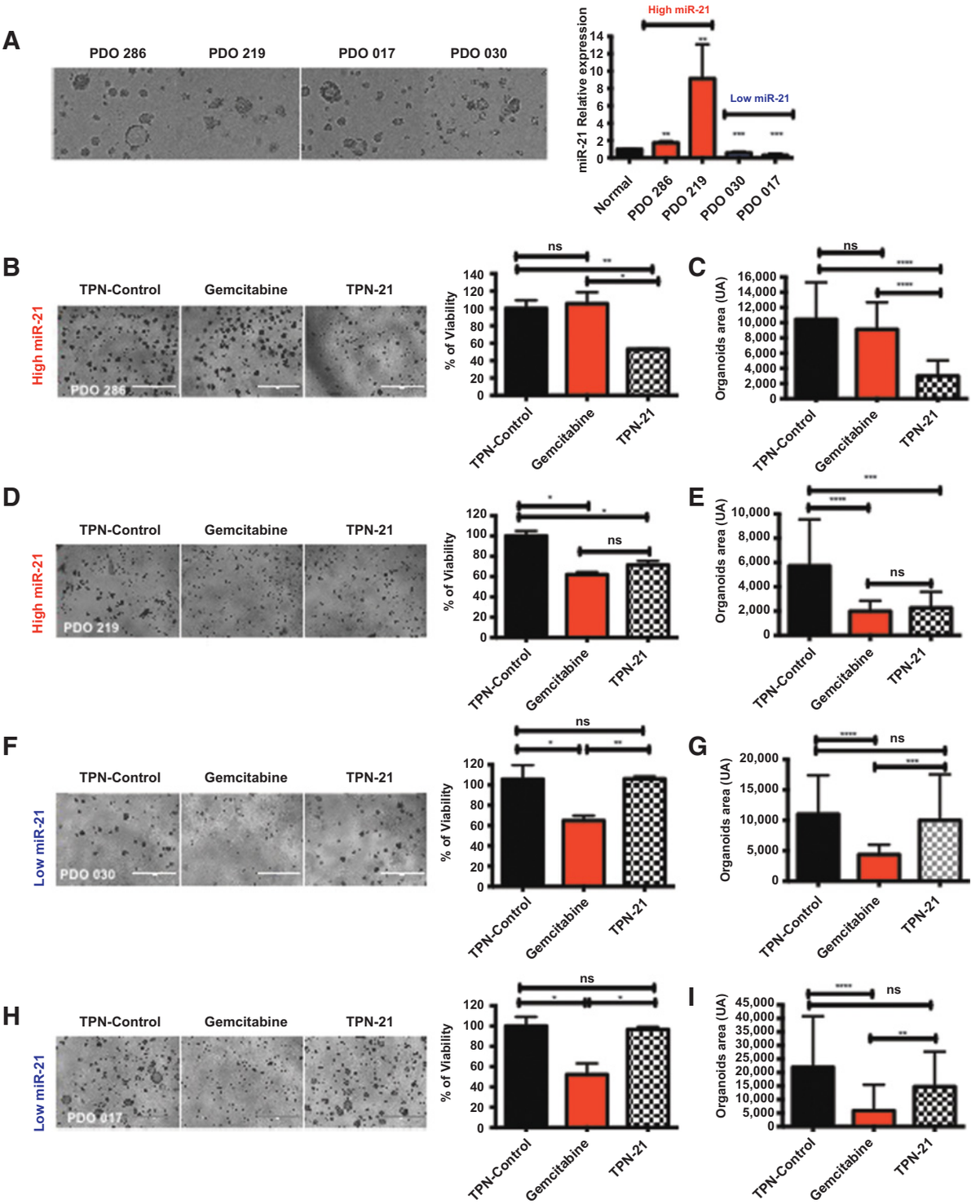

Figure 6.

A, Representative pictures and qPCR analysis of miR-21-5p expression levels in 4 PDO (Panc 286, Panc 219, PDO 030, and PDO 017). Scale bar, 1,000 μm. **B, D**, **F**, and **H,** PDO metabolic activity measured from MTT assay after repeated TPN-21 treatments and representative pictures of PDO 286, PDO 219, PDO 030, and PDO 017. Scale bar, 1,000 μm. **C, E, G,** and **I,** Quantification of organoid size after TPN-21 treatment. Organoids size was measured through ImageJ software on a total of 35 spheroids and is presented in arbitrary units (UA). For qPCR, each miRNA sample was normalized on the basis of its 18s content. *, $P = 0.01$–0.05; **, $P = 0.001$–0.01; ***, $P < 0.001$; ****, $P < 0.0001$; N.S., not significant, two-tailed *t* test.

Published OnlineFirst January 12, 2018; DOI: 10.1158/1078-0432.CCR-17-2733

guide precision medicine are emerging (33, 38–40). In this study, through the utilization of PDO as a rapid screen for TPN-21, we show for the first time the potential of personalized models for RNA-based precision medicine therapy in PDAC. By working with patient avatars, we have shown the potential to harness the ability of PDO and PDX models to predict clinical outcomes of patients and thus align preclinical work to patient response to TPN-21 therapy, a key goal in personalized medicine (41).

Our work reveals that for PDAC, miR-21 is both a companion diagnostic and the therapeutic target, a theranostic. Upregulation of miR-21 in tumor and stromal tissues is currently clearly associated with several gastrointestinal tumor types (pancreatic cancer, esophageal, gastric cancer, liver cancer; refs. 42, 43) and resistance to multiple anticancer agents (44) and is a promising noninvasive biomarker for pancreatic cancer risk and detection (24, 45, 46). As miR-21 is already a key detectable biomarker for PDAC (27, 47, 48), in a future phase I clinical trial, we propose to prospectively identify patients presenting with a similar miRNA signature that could be eligible for this biomarker-based RNA therapy.

In the near future, additional antimiRs (and miRNA mimics) could be packaged into the TPN system and tested on PDO, including the 3 key miRNAs deregulated from our PDAC profiling (TPN-7i, TPN-196a, TPN-196b for anti-let-7i, anti-miR-196a, and anti-miR-196b). Use of miRNA-based therapy for PDAC treatment is very novel and is positioned at the forefront of current PDAC and RNA medicine therapeutic challenges. This general approach, described here through this successful proof of principle using anti-miR-21 theranotics, shows very high potential not only for clinical significance but in the establishment of integrative screening methodologies with broad applicability to other cancers and lethal diseases with notoriously dismal clinical outcome.

Materials and Methods

miRNA profiling

For miRNA analysis, total RNA was isolated from frozen PDX tissue samples using the mirVana miRNA Isolation Kit following standard protocol (Invitrogen). Total RNA samples were sent to Abcam Firefly group for miRNAs Firefly analysis. Data analysis and plotting heatmap and volcano plots were done through Firefly Analysis Workbench software for multiplex miRNA assays. For PDX tissue sample data analysis, miRNAs were normalized using miR-22-3p and miR-30b-5p and were defined by the geNorm-like algorithm. For cell lines, 3D model, and organoids, miRNAs were normalized using miR-181b-5p, miR-103-3p, and miR-30b-5p, which were defined by the geNorm-like algorithm.

Tumor mouse models

For generation of PDX mouse models, tumor organoids were grown in 3D tissue culture for 16 days and then dissociated with collagenase/dispase, Accutase. Dissociated cells were resuspended in organoid growth media supplemented with 50% Matrigel and 10 μmol/L Y27632 at final concentration 2.5×10^6 cells/mL, and the suspension was kept on ice all the time. Six-week-old nude mice were injected with 100 μL cell suspension on to the right flank of each mouse. Tumor growth was monitored twice a week by observation and palpation. We defined approximately 100 mm^3 tumors as the starting point to perform a treatment trial. Mice were treated 2 times a week for a total of 4 intravenous injections with either TPN-21 or TPN-control (5 mg/kg oligonucleotides) or saline solution as an additional control. At the end of the treatment, mice were sacrificed, tumors were collected, and samples were processed appropriately. All procedures were conducted following an institutionally approved animal IACUC protocol. We conducted therapeutic trials in a subcutaneous model of pancreatic cancer driven by D8-175 cell line. Bilateral flank allografts were implanted on 6-week-old NCR/nude mice each seeded with 5×10^5 cells. Mice were divided into groups of 5, with nearly equal average and standard deviation of tumor burden at the start of treatment (~150 mm^3 total tumor burden per mouse). TPN-21 or TPN-control (5 mg/kg oligonucleotides) or saline solution was administrated intravenously twice every week until the tumor burden reached or exceeded 1 cm according to the approved animal operation protocol. For biodistribution study, D8-175 cells carrying stably expressed luciferase were suspended in PBS and directly injected into the parenchyma of pancreatic tails of nude mice (5–6 weeks) at 5×10^5 cells in 100 μL per mouse. The rate of tumor formation was tracked using IVIS system every week after surgical operation. To investigate biodistribution of TPNs in this orthotopic PDAC model, 100 μL of fluorescence labeled nanoparticles (TAMRA-TPN-21) carrying 7.5 μmol/L of miR-21 antagonists were injected through intravenous administration into tumor-bearing mice. Four hours after TAMRA-TPN-21 injection, mice were scarified; major organs (liver, spleen, lung, kidney, hear, tumor) were extracted and scanned using a LI-COR Odyssey Near-Infrared Imaging System. Fluorescence intensity of each organ was measured and quantified using ImageJ.

qPCR

3D models and organoids were separated from Matrigel by washing with PBS. Cell lines, 3D models, and organoids were lysed using TRIzol, and RNA extraction was done using the mirVana miRNA Isolation Kit. cDNA synthesis was performed using miScript II RT Kit (Qiagen) with 250 ng RNA as input. qRT-PCR was performed using the Roche480 Light Cycler miRNA system as per the manufacturer's instructions, and gene expression was normalized to U6 and/or 18s. For mRNA analysis, cDNA synthesis was performed using Verso cDNA Synthesis Kit (Life Technologies) using 500 to 1,000 ng RNA as input. cDNA was used for SYBR Green–based real-time PCR. Gene expression was normalized to GAPDH and or β-actin. Hsa-miR-21-5p and U6 miScript Primer and 18s, MMP-2, MMP-9, GAPDH, β-actin, PTEN, and PDCD4 QuantiTect Primer are from Qiagen.

Cell lines and antimiR transfection

PANC-1, PL-45, BxPC3, and Capan-2 were obtained from the ATCC and cultured at 37°C with 5% CO_2 in DMEM, RPMI1640, and McCoy's 5a Medium Modified supplemented with 10% FBS and 1% penicillin/streptomycin. H6c7 (human pancreatic duct epithelial cell line) and ECA001 were obtained from Kerafast and maintained in Keratinocyte Basal Medium + supplied supplements (Lonza, Clonetics KBM, cat#CC-3111). D8-175 is a cell line derived from Pdx1-Cre; $Kras^{+/LSL\text{-}G12D}$; $Trp53^{fl/fl}$ (KPC) mice and was cultured in DMEM supplemented with 10% FBS and 1% penicillin/streptomycin. Cell lines were tested for mycoplasma using the Lonza MycoAlert Detection Kit. For RNA-based functional experiments, mirVana miRNA inhibitor for hsa-miR-21-5p and mirVana miRNA Inhibitor, negative control #1 (Life Technologies) was used at 50 nmol/L and transfected into cells using RNAiMAX (invitrogen), as per the manufacturer's protocol.

Published OnlineFirst January 12, 2018; DOI: 10.1158/1078-0432.CCR-17-2733

3D models and organoids

Snap-frozen PDAC tumor samples used in this work were obtained from the M. Hidalgo's PDX collection. The pancreatic cancer PDXs were generated as described in refs. 10 and 25. The *KRAS* mutational status and sensitivity to gemcitabine were routinely analyzed for most of the PDX models within the collection. To generated PDAC 3D cell culture models, 2,000 PANC-1 or BxPC3 cells were mixed with Geltrex Matrix (Thermo Fisher Scientific) and DMEM or RPMI1640 medium supplemented with 10% FBS and 1% penicillin/streptomycin as 1/1 ratio and plated on nontissue culture treated 96-well plates (BD Falcon). After the matrix solidified, 100 μL medium was added on the well, and spheroids were grown under standard culture conditions (5% CO_2, at 37°C). Normal human pancreatic progenitors were derived from human pluripotent stem cells through a two-stage induction protocol, in DMEM based media including B27, insulin, hydrocortisone, and other factors, as described previously (33). Tumor organoids and PDX mouse models were generated as described by Huang and colleagues (2015). Fresh PDX tumor fragments were minced with a no. 22 blade into 1 to 2 mm small pieces then digested with 1 mg/mL collagenase/dispase for 30 minutes, follow by Accutase digestion for 40 minutes. The slurry was resuspended in DMEM and then filtered through a tissue strainer and centrifuged at 1,500 rpm for 5 minutes. After aspirating the supernatant, we resuspended the cell pellet with organoid growth medium supplemented with 5% Matrigel and 10 μmol/L Y27632. Organoids were grown under standard culture conditions (5% CO_2, at 37°C).

To perform a dose–response study, organoids were treated with TPN-21, TPN-control, or gemcitabine (HCL, Calbiochem; 12.5, 25, 50, and 100 nmol/L) following an every-other-day treatment plan. Organoids were tested with gemcitabine at 100 nmol/L alone or combined with TPN-21 following an every-other-day treatment plan.

Histology and image acquisition

For histologic evaluation, 3D models and organoids were fixed with 4% PFA and embedded in paraffin. Embedding, sectioning, and H&E were processed by the Histology Core of Beth Israel Deaconess Medical Center (Boston, MA). IHC of integrins [anti-integrin alpha V antibody (Abcam 179475, 1: 1,000)] and NRP1 [anti-NRP-1 (Abcam 81321, 1: 300)] was performed in histology core at the Swanson Biotechnology Center of Koch Institute (Cambridge, MA).

Phase-contrast and fluorescent images were acquired on a EVOS FL Cell Imaging System with a 4×, 10×, or 20× objective. Analysis of number of 3D models and organoids after TPN-control or TPN-21 treatments was conducted on >3 independents well per conditions in each experiment for >3 independent experiments. Confocal images of 3D models were acquired with the Zeiss LSM 510 Inverted Live-Cell Confocal System using 20× Zeiss Apochromat dry, 0.8 NA at the Confocal Imaging Core of Beth Israel Deaconess Medical Center. All experiments were conducted with >30 structures evaluated in each experiment.

Generation of stable cell lines

To generate the stable pLenti-III-miR-21-off (Lenti-21) line, 2,000 PANC-1 cells were seeded in a 96-well plate in DMEM supplemented with 10% FBS. Twenty-four hours later, PANC-1 was cotransfected with LentimiRa-Off-hsa-miR-21-5p virus (abm) or Lenti-III-mir-Off control virus (abm) at MOI 5 in the presence of polybrene 8 μg/μL (SIGMA) and Virusplus 1/100 (abm). After 24 hours of incubation, medium was replaced with fresh medium for another 24 hours before selection of stable GFP-positive transductants in media containing 1.5 μg/mL of puromycin for 3 days.

Viability and apoptotic assay

Viability assay on 3D models was performed by using MTT reagents from SIGMA (M2128) according to the manufacturer's recommendations. The apoptosis assay was performed by using NucView 530 Caspase-3 Substrate (Biotium). Briefly 3D models were incubated with NucView reagent (1/500) and Hoescht (1/1,000) for 30 to 60 minutes, and the red signal corresponding to caspase-3–positive structures was counted and normalized to the total number of structures. Viability and apoptosis of 3D models and organoids after treatment was conducted on >3 independents well per condition in each experiment for >3 independent experiments.

Western blotting

The H6c7 normal pancreatic cell line and PDAC human and mouse cell lines were cultured and lysed in 1× RIPA buffer with protease and phosphatase inhibitor (Thermo Fisher Scientific) for 30 minutes on ice. The whole-cell lysates were then clarified by centrifugation for 25 minutes at 15,000 rpm at 4°C. Protein concentrations were determined using the BCA Protein Assay Kit (Pierce). Equal amounts (10 μg) of protein samples were fractionated by a Novex 4% to 20% Tris-Glycine gel (Thermo Fisher Scientific), transferred to nitrocellulose membranes (Thermo Fisher Scientific), and blocked in Odyssey blocking buffer (LI-COR Biosciences). Integrin was probed by primary rabbit antibody (1:1,000; Abcam, ab52971), NRP-1 was stained using primary rabbit antibody (1:500) (Abcam, ab81321), and tubulin was measured using primary rabbit antibody (Cell Signaling Technology, #2144). The desired bands were detected by labeling with anti-rabbit (1:10,000) IgG–IRDye 680 secondary antibodies and visualized using the Odyssey Infrared Imaging System (LI-COR Biosciences).

TPN and binding assay

All peptides in this study are produced by solid-phase peptide synthesis CPC Scientific. Tandem peptide (pTP-iRGD) has the sequence CH3(CH)15-GWTLNSAGYLLGKINLKALAALAKKIL-GGK(TAMRA)GGCRGDKGPDC; Cys-Cys bridge was synthesized by CPC Scientific. mirVana miRNA inhibitor against hsa-miR-21-5p and nontargeting controls were obtained from Thermo Fisher Scientific. PEGylation method of the tandem peptide was described previously (49).To form the TPNs in solution, miRNA inhibitor, PEGylated pTP-iRGD, and pTP-iRGD were resuspended in nuclease-free water and mixed with the miRNA inhibitor, PEG-containing component, and peptide in 1:2.5:15 molar ratios, first by thoroughly mixing the miRNA with the PEGylated pTP-iRGD and by subsequently mixing in the peptide to create a concentrated solution of TPNs that were adjusted to the desired dilution and buffer composition with appropriate diluent. Binding of iRGD-TAMRA on cells was done at 4°C on ice. The H6c7 normal pancreatic cell line and PDAC human and mouse cell lines (PANC1 and D8-175) were placed for 30 minutes on ice before addition of iRGD-TAMRA (10 nmol/L). After 15-minute treatment with iRGD-TAMRA, cells were washed 3 times with PBS and fixed with 4% PFA and stained with DAPI.

Published OnlineFirst January 12, 2018; DOI: 10.1158/1078-0432.CCR-17-2733

Statistical Analysis

Statistical analysis was achieved by using a two-tailed unpaired *t* test using GraphPad Prism software. Two-way ANOVA has been done for miRNA profiling assays. All graphs show means ± SD (*, $P = 0.01–0.05$; **, $P = 0.001–0.01$; ***, $P < 0.001$; ****, $P < 0.0001$; N.S., not significant). For qRT-PCR data, means and SD were calculated at the ddC_t level before being converted to fold changes as presented in the graphs (50).

Disclosure of Potential Conflicts of Interest

No potential conflicts of interest were disclosed.

Authors' Contributions

Conception and design: M.-E. Gilles, L. Hao, E. Pulver, M. Hidalgo, S.N. Bhatia, F.J. Slack

Development of methodology: M.-E. Gilles, L. Hao, L. Huang, F.J. Slack

Acquisition of data (provided animals, acquired and managed patients, provided facilities, etc.): M.-E. Gilles, L. Hao, R. Rupaimoole, E. Pulver, M. Hidalgo

Analysis and interpretation of data (e.g., statistical analysis, biostatistics, computational analysis): M.-E. Gilles, L. Hao, J.C. Jeong

Writing, review, and/or revision of the manuscript: M.-E. Gilles, L. Hao, L. Huang, P.P. Lopez-Casas, S.K. Muthuswamy, M. Hidalgo, S.N. Bhatia, F.J. Slack

Administrative, technical, or material support (i.e., reporting or organizing data, constructing databases): M.-E. Gilles, L. Huang, R. Rupaimoole, P.P. Lopez-Casas, E. Pulver

Study supervision: M.-E. Gilles, S.N. Bhatia, F.J. Slack

Other (provided intellectual and technical assistance with the use of tumor organoid platform): S.K. Muthuswamy

Acknowledgments

We thank Heather Fleming and Teddy Jégu for critical reading of this manuscript, Omar Gandarilla Cuellar and Dipikaa Ashinthala for providing PDO and reagents required for PDO growth, and Nelson Moreira for providing normal pancreatic tissue samples. This work was supported by a grant to F.J. Slack and S.N. Bhatia by the Harvard Medical School Initiative for RNA Medicine and to F.J. Slack, S.K. Muthuswamy, and M. Hidalgo from the BIDMC CAO Pilot Award.

The costs of publication of this article were defrayed in part by the payment of page charges. This article must therefore be hereby marked *advertisement* in accordance with 18 U.S.C. Section 1734 solely to indicate this fact.

Received September 18, 2017; revised November 21, 2017; accepted January 3, 2018; published OnlineFirst January 12, 2018.

References

1. Hidalgo M, Cascinu S, Kleeff J, Labianca R, Lohr JM, Neoptolemos J, et al. Addressing the challenges of pancreatic cancer: future directions for improving outcomes. Pancreatology 2015;15:8–18.
2. Rachagani S, Macha MA, Menning MS, Dey P, Pai P, Smith LM, et al. Changes in microRNA (miRNA) expression during pancreatic cancer development and progression in a genetically engineered KrasG12D; Pdx1-Cre mouse (KC) model. Oncotarget 2015;6:40295–309.
3. Muller S, Raulefs S, Bruns P, Afonso-Grunz F, Plotner A, Thermann R, et al. Next-generation sequencing reveals novel differentially regulated mRNAs, lncRNAs, miRNAs, sdRNAs and a piRNA in pancreatic cancer. Mol Cancer 2015;14:94.
4. Giovannetti E, Funel N, Peters GJ, Del Chiaro M, Erozenci LA, Vasile E, et al. MicroRNA-21 in pancreatic cancer: correlation with clinical outcome and pharmacologic aspects underlying its role in the modulation of gemcitabine activity. Cancer Res 2010;70:4528–38.
5. The Cancer Genome Atlas Research Network. Electronic address aadhe, Cancer Genome Atlas Research N. integrated genomic characterization of pancreatic ductal adenocarcinoma. Cancer Cell 2017;32:185–203.
6. Medina PP, Nolde M, Slack FJ. OncomiR addiction in an *in vivo* model of microRNA-21-induced pre-B-cell lymphoma. Nature 2010;467:86–90.
7. Cheng CJ, Bahal R, Babar IA, Pincus Z, Barrera F, Liu C, et al. MicroRNA silencing for cancer therapy targeted to the tumour microenvironment. Nature 2015;518:107–10.
8. Rupaimoole R, Slack FJ. MicroRNA therapeutics: towards a new era for the management of cancer and other diseases. Nat Rev Drug Discov 2017;16:203–22.
9. Gilles ME, Maione F, Cossutta M, Carpentier G, Caruana L, Di Maria S, et al. Nucleolin targeting impairs the progression of pancreatic cancer and promotes the normalization of tumor vasculature. Cancer Res 2016;76:7181–93.
10. Diamantopoulou Z, Gilles ME, Sader M, Cossutta M, Vallée B, Houppe C, et al. Multivalent cationic pseudopeptide polyplexes as a tool for cancer therapy. Oncotarget 2017;8:90108–22.
11. Wu SY, Lopez-Berestein G, Calin GA, Sood AK. RNAi therapies: drugging the undruggable. Sci Transl Med 2014;6:240ps7.
12. Sicard F, Gayral M, Lulka H, Buscail L, Cordelier P. Targeting miR-21 for the therapy of pancreatic cancer. Mol Ther 2013;21:986–94.
13. Zhao G, Wang B, Liu Y, Zhang JG, Deng SC, Qin Q, et al. miRNA-141, downregulated in pancreatic cancer, inhibits cell proliferation and invasion by directly targeting MAP4K4. Mol Cancer Ther 2013;12:2569–80.
14. Tu MJ, Pan YZ, Qiu JX, Kim EJ, Yu AM. MicroRNA-1291 targets the FOXA2-AGR2 pathway to suppress pancreatic cancer cell proliferation and tumorigenesis. Oncotarget 2016;7:45547–61.
15. Hou BH, Jian ZX, Cui P, Li SJ, Tian RQ, Ou JR. miR-216a may inhibit pancreatic tumor growth by targeting JAK2. FEBS Lett 2015;589:2224–32.
16. Pramanik D, Campbell NR, Karikari C, Chivukula R, Kent OA, Mendell JT, et al. Restitution of tumor suppressor microRNAs using a systemic nanovector inhibits pancreatic cancer growth in mice. Mol Cancer Ther 2011;10:1470–80.
17. Teesalu T, Sugahara KN, Ruoslahti E. Tumor-penetrating peptides. Front Oncol 2013;3:216.
18. Sugahara KN, Teesalu T, Karmali PP, Kotamraju VR, Agemy L, Girard OM, et al. Tissue-penetrating delivery of compounds and nanoparticles into tumors. Cancer Cell 2009;16:510–20.
19. Sugahara KN, Braun GB, de Mendoza TH, Kotamraju VR, French RP, Lowy AM, et al. Tumor-penetrating iRGD peptide inhibits metastasis. Mol Cancer Ther 2015;14:120–8.
20. Ren Y, Hauert S, Lo JH, Bhatia SN. Identification and characterization of receptor-specific peptides for siRNA delivery. ACS Nano 2012;6:8620–31.
21. Ren Y, Sagers JE, Landegger LD, Bhatia SN, Stankovic KM. Tumor-Penetrating Delivery of siRNA against TNFalpha to Human Vestibular Schwannomas. Sci Rep 2017;7:12922.
22. Liu X, Lin P, Perrett I, Lin J, Liao YP, Chang CH, et al. Tumor-penetrating peptide enhances transcytosis of silicasome-based chemotherapy for pancreatic cancer. J Clin Invest 2017;127:2007–18.
23. Byrne AT, Alferez DG, Amant F, Annibali D, Arribas J, Biankin AV, et al. Interrogating open issues in cancer precision medicine with patient-derived xenografts. Nat Rev Cancer 2017;17:254–68.
24. Rubio-Viqueira B, Jimeno A, Cusatis G, Zhang X, Iacobuzio-Donahue C, Karikari C, et al. An in vivo platform for translational drug development in pancreatic cancer. Clin Cancer Res 2006;12:4652–61.
25. Garrido-Laguna I, Uson M, Rajeshkumar NV, Tan AC, de Oliveira E, Karikari C, et al. Tumor engraftment in nude mice and enrichment in stroma- related gene pathways predict poor survival and resistance to gemcitabine in patients with pancreatic cancer. Clin Cancer Res 2011;17:5793–800.
26. Goswami CP, Nakshatri H. PROGmiR: a tool for identifying prognostic miRNA biomarkers in multiple cancers using publicly available data. J Clin Bioinforma 2012;2:23.

27. Frampton AE, Krell J, Jamieson NB, Gall TM, Giovannetti E, Funel N, et al. microRNAs with prognostic significance in pancreatic ductal adenocarcinoma: A meta-analysis. Eur J Cancer 2015;51:1389–404.
28. Ali S, Almhanna K, Chen W, Philip PA, Sarkar FH. Differentially expressed miRNAs in the plasma may provide a molecular signature for aggressive pancreatic cancer. Am J Transl Res 2010;3:28–47.
29. Moriyama T, Ohuchida K, Mizumoto K, Yu J, Sato N, Nabae T, et al. MicroRNA-21 modulates biological functions of pancreatic cancer cells including their proliferation, invasion, and chemoresistance. Mol Cancer Ther 2009;8:1067–74.
30. Ruoslahti E. Tumor penetrating peptides for improved drug delivery. Adv Drug Deliv Rev 2016;110–111:3–12.
31. White PJ, Anastasopoulos F, Pouton CW, Boyd BJ. Overcoming biological barriers to in vivo efficacy of antisense oligonucleotides. Exp Rev Mol Med 2009;11:e10.
32. Hingorani SR, Wang L, Multani AS, Combs C, Deramaudt TB, Hruban RH, et al. Trp53R172H and KrasG12D cooperate to promote chromosomal instability and widely metastatic pancreatic ductal adenocarcinoma in mice. Cancer Cell 2005;7:469–83.
33. Huang L, Holtzinger A, Jagan I, BeGora M, Lohse I, Ngai N, et al. Ductal pancreatic cancer modeling and drug screening using human pluripotent stem cell- and patient-derived tumor organoids. Nat Med 2015; 21:1364–71.
34. Li Y, Chen Y, Li J, Zhang Z, Huang C, Lian G, et al. Co-delivery of microRNA-21 antisense oligonucleotides and gemcitabine using nanomedicine for pancreatic cancer therapy. Cancer Sci 2017;108:1493–503.
35. Zhang J, Jiao J, Cermelli S, Muir K, Jung KH, Zou R, et al. miR-21 inhibition reduces liver fibrosis and prevents tumor development by inducing apoptosis of CD24+ progenitor cells. Cancer Res 2015;75:1859–67.
36. Wagenaar TR, Zabludoff S, Ahn SM, Allerson C, Arlt H, Baffa R, et al. Anti-miR-21 suppresses hepatocellular carcinoma growth via broad transcriptional network deregulation. Mol Cancer Res 2015;13:1009–21.
37. Chau BN, Xin C, Hartner J, Ren S, Castano AP, Linn G, et al. MicroRNA-21 promotes fibrosis of the kidney by silencing metabolic pathways. Sci Transl Med 2012;4:121ra18.
38. Pauli C, Hopkins BD, Prandi D, Shaw R, Fedrizzi T, Sboner A, et al. Personalized in vitro and in vivo cancer models to guide precision medicine. Cancer Discov 2017;7:462–77.
39. Baker LA, Tiriac H, Clevers H, Tuveson DA. Modeling pancreatic cancer with organoids. Trends Cancer 2016;2:176–90.
40. Broutier L, Andersson-Rolf A, Hindley CJ, Boj SF, Clevers H, Koo BK, et al. Culture and establishment of self-renewing human and mouse adult liver and pancreas 3D organoids and their genetic manipulation. Nat Protoc 2016;11:1724–43.
41. Perales-Paton J, Pineiro-Yanez E, Tejero H, Lopez-Casas PP, Hidalgo M, Gomez-Lopez G, et al. Pancreas cancer precision treatment using avatar mice from a bioinformatics perspective. Public Health Genomics 2017; 20:77–87.
42. Tazawa H, Kagawa S, Fujiwara T. MicroRNAs as potential target gene in cancer gene therapy of gastrointestinal tumors. Exp Opin Biol Ther 2011; 11:145–55.
43. Kadera BE, Li L, Toste PA, Wu N, Adams C, Dawson DW, et al. MicroRNA-21 in pancreatic ductal adenocarcinoma tumor-associated fibroblasts promotes metastasis. PLoS One 2013;8:e71978.
44. Feng YH, Tsao CJ. Emerging role of microRNA-21 in cancer. Biomed Rep 2016;5:395–402.
45. Qu K, Zhang X, Lin T, Liu T, Wang Z, Liu S, et al. Circulating miRNA-21–5p as a diagnostic biomarker for pancreatic cancer: evidence from comprehensive miRNA expression profiling analysis and clinical validation. Sci Rep 2017;7:1692.
46. Yuan W, Tang W, Xie Y, Wang S, Chen Y, Qi J, et al. New combined microRNA and protein plasmatic biomarker panel for pancreatic cancer. Oncotarget 2016;7:80033–45.
47. Duell EJ, Lujan-Barroso L, Sala N, Deitz McElyea S, Overvad K, Tjonneland A, et al. Plasma microRNAs as biomarkers of pancreatic cancer risk in a prospective cohort study. Int J Cancer 2017;141:905–15.
48. Jamieson NB, Morran DC, Morton JP, Ali A, Dickson EJ, Carter CR, et al. MicroRNA molecular profiles associated with diagnosis, clinicopathologic criteria, and overall survival in patients with resectable pancreatic ductal adenocarcinoma. Clin Cancer Res 2012;18:534–45.
49. Lo JH, Kwon EJ, Zhang AQ, Singhal P, Bhatia SN. Comparison of Modular PEG incorporation strategies for stabilization of peptide-siRNA nanocomplexes. Bioconjug Chem 2016;27:2323–31.
50. Livak KJ, Schmittgen TD. Analysis of relative gene expression data using real-time quantitative PCR and the 2(-Delta Delta C(T)) Method. Methods 2001;25:402–8.

Published OnlineFirst January 12, 2018; DOI: 10.1158/1078-0432.CCR-17-2733

Clinical Cancer Research

Personalized RNA Medicine for Pancreatic Cancer

Maud-Emmanuelle Gilles, Liangliang Hao, Ling Huang, et al.

Clin Cancer Res 2018;24:1734-1747. Published OnlineFirst January 12, 2018.